



Disulfide isomerase activity of the dynamic, trimeric *Proteus mirabilis* ScsC protein is primed by the tandem immunoglobulin-fold domain of ScsB

Received for publication, January 12, 2018, and in revised form, February 15, 2018. Published, Papers in Press, February 28, 2018, DOI 10.1074/jbc.RA118.001860

Emily J. Furlong^{‡§}, Hassanul G. Choudhury^{‡1}, Fabian Kurth^{‡2}, Anthony P. Duff[¶], Andrew E. Whitten^{¶13}, and Jennifer L. Martin^{‡§4}

From the [‡]Institute for Molecular Bioscience, University of Queensland, St. Lucia, Queensland 4072, Australia, [§]Griffith Institute for Drug Discovery, Griffith University, Nathan, Queensland 4111 Australia, and [¶]Australian Nuclear Science and Technology Organisation, Lucas Heights, New South Wales 2234, Australia

Edited by Norma M. Allewell

Correct disulfide bond formation is essential for proper folding of many proteins, including bacterial virulence factors. The suppressor of copper sensitivity (Scs) proteins have roles in dithiol/disulfide interchange and the bacterial response to copper stress. Encoded in a four-gene cassette (ScsABCD) present in many Gram-negative bacteria, the Scs proteins are enigmatic and poorly characterized. Here, we show that the periplasmic α -domain of the membrane protein ScsB in the Gram-negative bacterium *Proteus mirabilis* forms a redox relay with the soluble periplasmic protein PmScsC. We also found that the periplasmic α -domain is sufficient to activate the disulfide isomerase activity of PmScsC. The crystal structure of PmScsB α at a resolution of 1.54 Å revealed that it comprises two structurally similar immunoglobulin-like folds, one of which includes a putative redox-active site with the sequence CXXXC. We confirmed the importance of these cysteine residues for PmScsB α function, and in addition, we engineered cysteine variants that produced a stable complex between PmScsC and PmScsB α . Using small-angle X-ray and neutron scattering analyses with contrast variation, we determined a low-resolution structure of the PmScsC–PmScsB α complex. The structural model of this complex suggested that PmScsB α uses both of its immunoglobulin-like folds to interact with PmScsC and revealed that the highly dynamic PmScsC becomes ordered upon PmScsB α binding. These findings add to our understanding of the poorly characterized Scs proteins.

This work was supported by Australian Research Council Laureate Fellowship FL0992138 (to J. L. M.), Australian Research Council Discovery Project DP130100576 (to J. L. M.; H. G. C. salary), an Australian postgraduate award (to E. J. F.), and an Institute for Molecular Bioscience research advancement award (to E. J. F.). The authors declare that they have no conflicts of interest with the contents of this article.

This article was selected as one of our Editors' Picks.

The atomic coordinates and structure factors (code 6C29) have been deposited in the Protein Data Bank (<http://wwpdb.org/>).

SAXS/SANS data and the model of the 3:1 PmScsC–PmScsB α complex have been submitted to the Small Angle Scattering Biological Data Bank (SASBDB) under ID SASDC48.

¹ Present address: Cello Health Consulting, Farnham, Surrey GU9 7DN, United Kingdom.

² Present address: Bristol-Myers Squibb, Arnulfstrasse 29, 80636 Munich, Germany.

³ To whom correspondence may be addressed. E-mail: awh@ansto.gov.au.

⁴ To whom correspondence may be addressed: Griffith Institute for Drug Discovery, Griffith University, Nathan, Queensland 4111, Australia. E-mail: jl@griffith.edu.au.

The correct formation of disulfide bonds is an essential component in the folding of many proteins, including bacterial virulence factors. In bacteria, disulfide bond-forming (Dsb)⁵ proteins are responsible for introducing disulfide bonds into substrate proteins (DsbA and -B) (1, 2) as well as reducing and isomerizing (proofreading and shuffling) disulfide bonds that have been incorrectly introduced (DsbC and -D) (3, 4). Dsb proteins function through the redox action of two catalytic cysteines that are often embedded in a thioredoxin fold. These systems are well characterized in *Escherichia coli*; however, homologues of Dsb proteins exist in a range of Gram-negative bacteria. A group of related and poorly studied proteins found most commonly in Proteobacteria are the suppressor of copper sensitivity (Scs) proteins (5). The Scs proteins contribute to the bacterial virulence trait of resistance to copper stress (6, 7).

Originally identified in *Salmonella enterica* serovar Typhimurium (6), the *scs* locus encodes four proteins, ScsA–D, all of which have predicted catalytic motifs consisting of two cysteines (CXXC or CXXXC). Three of these (ScsB–D) incorporate a predicted thioredoxin fold, and one of the four (ScsA) has a predicted copper-binding motif. ScsD has a predicted N-terminal membrane anchor linked to a predicted periplasmic thioredoxin-fold domain (6) reminiscent of proteins involved in cytochrome *c* biogenesis, such as DsbE/CcmG (8, 9). The best studied of the four Scs proteins is the soluble periplasmic protein ScsC (5, 7, 10). An extraordinary feature is the variation in structure and function of ScsC proteins across different bacteria. *Caulobacter crescentus* ScsC (CcScsC) is reported to be a dimeric disulfide isomerase (5), *S. enterica* serovar Typhimurium ScsC (StScsC) is a monomeric redox protein with no disulfide isomerase activity (7), and *Proteus mirabilis* ScsC

⁵ The abbreviations used are: Dsb, disulfide bond-forming; Scs, suppressor of copper sensitivity; Pm, *P. mirabilis*; Cc, *C. crescentus*; St, *S. enterica* serovar Typhimurium; Ec, *E. coli*; r.m.s.d., root mean square deviation; SAXS, small-angle X-ray scattering; SANS, small-angle neutron scattering; WAXS, wide-angle X-ray scattering; AMS, 4-acetamido-4'-maleimidylstilbene-2,2'-disulfonic acid; SAD, single-wavelength anomalous diffraction; SEC, size exclusion chromatography; ^{99m}PmScsB α C114A, deuterium-labeled PmScsB α C114A; *p*(*r*), pair-distance distribution function; *I*(0), scattering intensity at zero angle; BisTris, 2-[bis(2-hydroxyethyl)amino]-2-(hydroxymethyl)propane-1,3-diol; scRNase A, scrambled RNase A; *R*_g, radius of gyration.

P. mirabilis ScsB α and ScsC form a functional redox relay

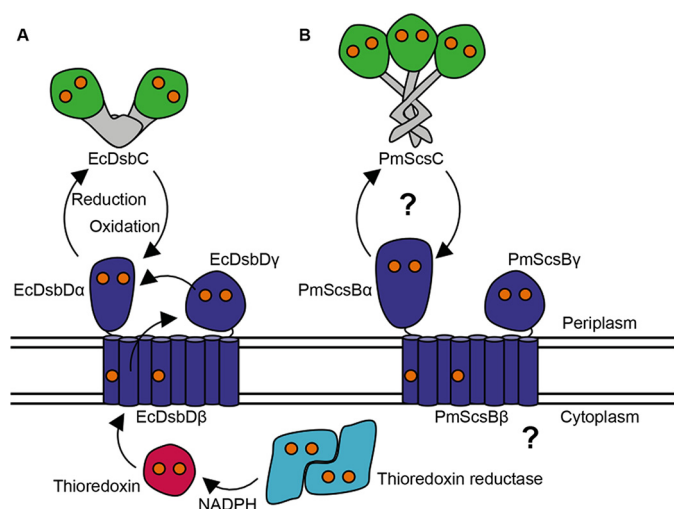


Figure 1. Schematic representation of bacterial disulfide isomerases and their redox relay partners. A, EcDsbC is reduced by EcDsbD α , which obtains its reducing power from a reduction cascade that starts with thioredoxin reductase in the bacterial cytoplasm. B, PmScsC and PmScsB α are putative interaction partners, and the source of PmScsB's reducing power is yet to be determined (represented by the question marks). The catalytic cysteines in each protein are shown as orange spheres.

(PmScsC) is a highly dynamic “shape-shifting” trimeric disulfide isomerase (10).

The present work focuses on the structure and function of *P. mirabilis* ScsB, a putative redox partner of *P. mirabilis* ScsC. ScsB resembles *E. coli* DsbD in many respects (5). EcDsbD is the membrane protein partner of the archetypal disulfide isomerase *E. coli* DsbC. Like EcDsbD, the ScsB protein is predicted to comprise three domains: an N-terminal periplasmic domain (DsbD α /ScsB α), a transmembrane domain (DsbD β /ScsB β) of eight helices, and a periplasmic C-terminal thioredoxin-fold domain (DsbD γ /ScsB γ) (Fig. 1, A and B). Each of the three domains in both EcDsbD and ScsB have two catalytic cysteine residues. In DsbD, these cysteine pairs in each domain form a reduction cascade that originates from thioredoxin reductase and NADPH in the cytoplasm, is passed through thioredoxin to DsbD β , DsbD γ , and then DsbD α , which reduces the cysteines in specific substrate proteins, such as DsbC (11, 12) (Fig. 1A). The similarity between the predicted architectures of EcDsbD and ScsB suggests the ScsB protein forms a similar redox relay system. Indeed, *C. crescentus* ScsB has been shown to interact with CcScsC and to maintain CcScsC in its reduced state, which is necessary for disulfide isomerase activity (5). A major difference between EcDsbD and ScsB is the size of their N-terminal α -domains. DsbD α comprises ~165 residues, whereas ScsB α is much larger at ~255 residues, and there is no detectable sequence identity between the α -domains of DsbD and ScsB. Because the α -domain of EcDsbD interacts directly with substrates, such as EcDsbC, the different size and sequence of the ScsB α -domain suggests that the proteins interact with different substrates (5).

In the present study, we investigated the structure and function of *P. mirabilis* ScsB α , showing that it forms a functional redox relay with the highly dynamic, trimeric disulfide isomerase PmScsC. We also report the first crystal structure of any ScsB α , revealing unexpectedly the presence of tandem immu-

noglobulin folds in PmScsB α and showing that this same arrangement is likely to be shared in ScsBs encoded by other organisms. We created a stable PmScsC–PmScsB α (trimer–monomer) complex and analyzed small-angle X-ray scattering (SAXS) data and small-angle neutron scattering (SANS) data with contrast variation to produce a low-resolution model of the complex. This model revealed that the highly dynamic PmScsC protein becomes more symmetric and ordered upon interaction with PmScsB α and that both immunoglobulin folds of PmScsB α interact with one protomer of PmScsC.

Results

PmScsC and PmScsB α form a specific redox relay system

From sequence analogy with CcScsB and CcScsC, PmScsB α is predicted to be the redox partner of PmScsC. If this functional relationship holds true, PmScsB α would specifically reduce oxidized PmScsC to convert it to the active reduced form. To confirm that a redox relay occurs between PmScsC and PmScsB α , we performed a redox gel-shift assay. First, we mixed PmScsC with PmScsB α and then analyzed the redox states of the two proteins after an incubation period. The redox state was defined by analyzing the proteins by SDS-PAGE after reaction with 4-acetamido-4'-maleimidylstilbene-2,2'-disulfonic acid (AMS) (Fig. 2A). When AMS binds to a reduced thiol, the mass is increased by 0.5 kDa, thus allowing discrimination between reduced and oxidized cysteine forms of a protein on mass-based gel separation. The results showed that when oxidized PmScsC was incubated with reduced PmScsB α , both proteins changed their redox states, confirming that disulfide exchange occurs between the two proteins (Fig. 2B). The reverse redox reaction did not occur: reduced PmScsC remained reduced when mixed with oxidized PmScsB α . Moreover, we were able to confirm the residues involved in the change in redox state because addition of the variant PmScsB α C114A to oxidized PmScsC did not catalyze disulfide exchange. However, there was some evidence for formation of a PmScsC–PmScsB α C114A complex (Fig. 2B, band marked X).

Control experiments using PmScsC or PmScsB α alone showed that, under the conditions of the experiment, these proteins did not spontaneously change their redox state. These results support the notion that PmScsC and PmScsB α form a specific redox relay system (Fig. 2B) and that the residues Cys¹¹⁴ and Cys¹¹⁸ of PmScsB α are responsible for the redox interaction.

PmScsB α primes the disulfide isomerase activity of PmScsC

We have previously shown that PmScsC is a disulfide isomerase (10). We tested the hypothesis that the redox interaction between PmScsB α and PmScsC might contribute to this function of PmScsC. We measured the disulfide isomerase activity of PmScsC using scrambled RNase A as substrate (Fig. 2A). Reduced PmScsC, but not oxidized PmScsC, was able to refold scrambled RNase A and thereby activate the enzyme (10) (Fig. 2C). PmScsB α on its own (oxidized or reduced) had no effect on the activity of scrambled RNase A. However, in the presence of reduced PmScsB α , the inactive oxidized PmScsC was able to restore the activity of RNase A. This result supports the hypothesis that PmScsB α reduces the disulfides of oxidized PmScsC,

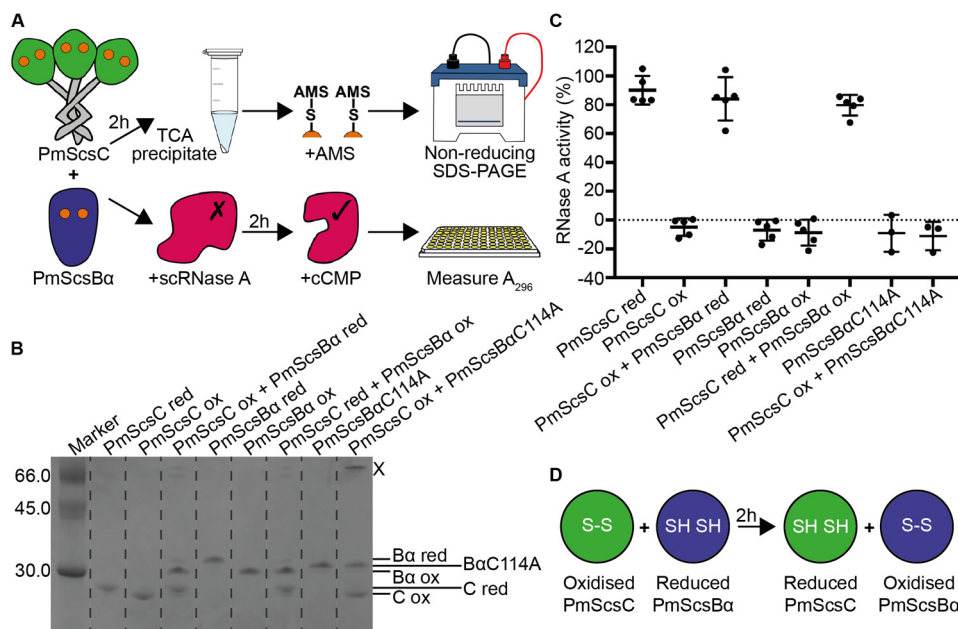


Figure 2. PmScsB α reduces and activates PmScsC. *A*, schematic diagrams of the gel-shift and scRNase A experiments. *B*, a representative gel from the gel-shift assay showing the interaction between PmScsC and PmScsB α . Dotted lines are a visual aide to delineate lanes on the gel. The band marked X is likely to be 1:1 PmScsC–PmScsB α C114A complex as the usually trimeric PmScsC runs as a monomer on SDS-PAGE. *C*, results from the modified scrambled RNase A assay. Activity is shown relative to native RNase A (100%) and scrambled RNase A only (0%) controls. For each sample, the activity of three or five replicates and the mean with S.D. (error bars) is shown. *D*, schematic showing the redox interaction that occurs between PmScsC and PmScsB α . red, reduced; ox, oxidized.

thereby enabling its disulfide isomerase activity (Fig. 2D). This experiment also confirmed that disulfide exchange in this system does not flow in the reverse direction: reduced PmScsC did not lose its ability to shuffle scrambled RNase A disulfides when it is incubated with oxidized PmScsB α . This may suggest that reduced PmScsC is unable to interact with PmScsB α . Furthermore, the cysteine variant in which Cys¹¹⁴ is mutated to Ala (PmScsB α C114A) does not activate oxidized PmScsC, showing that this cysteine is required for the redox relay to operate.

Crystal structure of PmScsB α

After removal of the periplasmic signal sequence, the predicted PmScsB α -domain comprises 255 residues (residues 21–275 of the reported PmScsB protein sequence, UniProt entry B4EV20). The crystal structure of this domain was solved to a resolution of 1.54 Å by using selenomethionine (SeMet)-labeled protein together with SAD phasing (Protein Data Bank code 6C29; Table 1 and Fig. 3, A–D). The structure revealed a monomer consisting of two immunoglobulin-like folds linked by an α -helix. This arrangement was consistent across all three molecules in the asymmetric unit (r.m.s.d., 0.7–1.0 Å, 247 residues aligned). Curiously, the two subdomains, A and B, are reasonably similar in structure (Fig. 3D; r.m.s.d., 2.5 Å, 81 residues aligned), although the sequence identity for such an alignment is very low (~7%). The subdomains each comprise two β -sheets, one with three β -strands and the other with four β -strands (Fig. 3, A and B). Subdomain A has additional features, including the cysteine motif (¹¹⁴CXXXC¹¹⁸), two β -strands forming a β -hairpin that links the two β -sheets of the canonical immunoglobulin fold, and a loop between β 2 and β 3 located on one side of the catalytic cysteines (Fig. 3D, arrows). The cysteines are present in the reduced form in all three molecules in the asymmetric unit.

Table 1
Crystallography statistics for PmScsB α

a/u, asymmetric unit; NA, not applicable.

	Protein Data Bank code 6C29 (SeMet)
Data collection	
Wavelength (Å)	0.9786
Resolution (Å)	97.06–1.538 (1.544–1.538) ^a
Space group	P2 ₁ 2 ₁ 2 ₁
Unit cell dimensions	
<i>a</i> , <i>b</i> , <i>c</i> (Å)	69.98, 97.06, 110.20
α , β , γ (°)	90, 90, 90
No. measured reflections	1,761,650
No. of unique reflections	111,511
<i>R</i> _{merge}	0.146 (2.114)
<i>R</i> _{p.i.m.}	0.038 (0.531)
Mean <i>I</i> / σ <i>I</i>	16.0 (2.1)
Redundancy	15.8 (16.3)
Completeness (%)	99.7 (98.3)
Wilson B	15.96
SAD phasing	
No. of sites	14
Figure of merit	0.42
Refinement	
No. of monomers in a/u	3
Resolution used in refinement (Å)	55.10–1.538
No. of reflections	111,388
<i>R</i> _{free} (%)	19.8
<i>R</i> _{work} (%)	17.3
No. of protein atoms	5,860
No. of ligand atoms	0
No. of waters	669
<i>B</i> factors (Å ²)	
Average	25.5
Protein atoms	24.8
Ligands	NA
Waters	31.8
r.m.s.d. bond length (Å)	0.011
r.m.s.d. bond angles (°)	1.332
Ramachandran favored/outlier (%)	97/0

^a Values in parentheses refer to the highest resolution shell.

The presence of an immunoglobulin-like fold in both PmScsB α subdomains resulted in many hits in a DALI search against the Protein Data Bank (13). Notably, the top hit was the

P. mirabilis ScsB α and ScsC form a functional redox relay

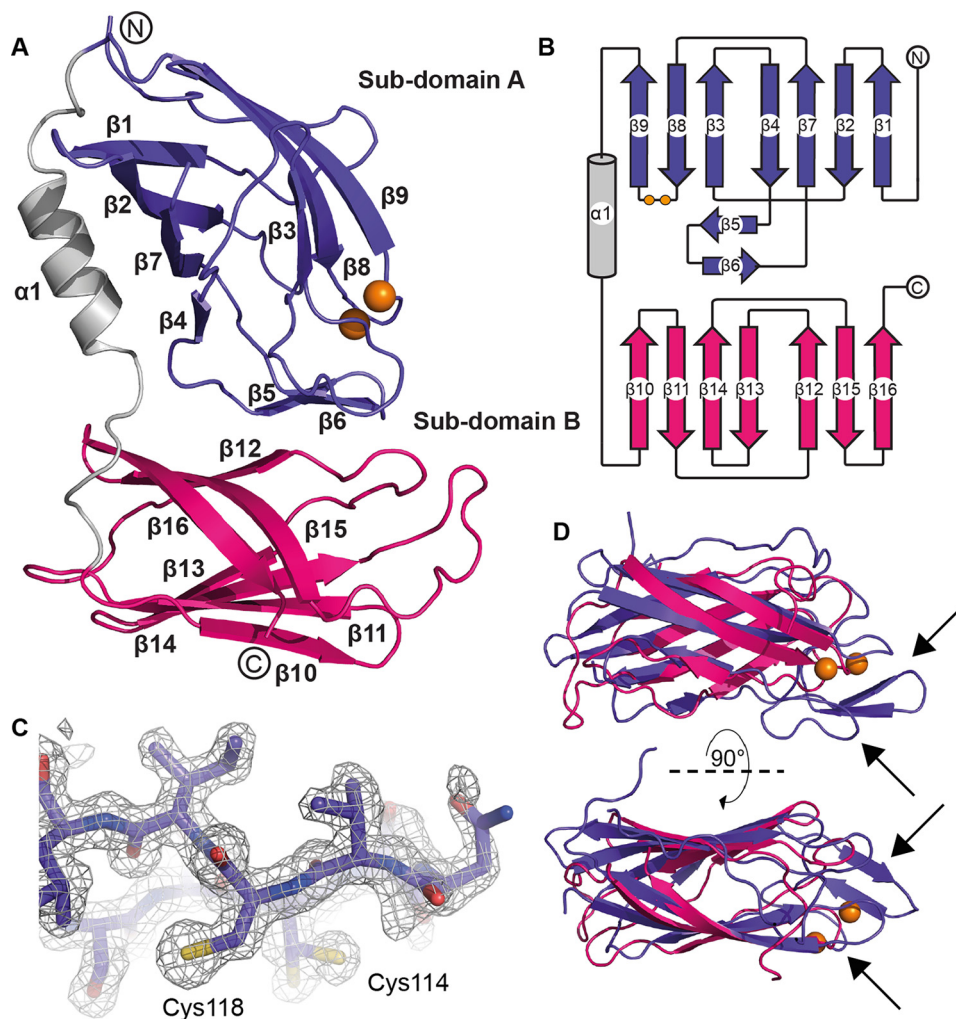


Figure 3. Structural characterization of PmScsB α . *A*, schematic representation of the crystal structure of PmScsB α (Protein Data Bank code 6C29). *B*, topology diagram of PmScsB α showing the secondary structure features of the protein. *C*, the omit electron density around the catalytic loop in chain A of the PmScsB α crystal structure is displayed. The wire mesh represents the likelihood-weighted $F_o - F_c$ electron density difference map, which is contoured to 3σ and was generated using phenix.refine with the region of interest omitted from the structure. *D*, superimposition of subdomain A and B structures showing the structural similarity between the domains. Arrows indicate the inserted β -hairpin structure and the extended loop of subdomain A. In all panels, subdomain A is colored purple, and subdomain B is magenta with the linking α -helix shown in gray. The catalytic cysteines are represented as orange spheres. The N and C termini are labeled in *A* and *B*.

functionally equivalent *E. coli* DsbD α (Protein Data Bank code 1JPE; r.m.s.d., 2.5 Å, 103 residues aligned), although it has only one immunoglobulin-like fold, which can be aligned with subdomain A of PmScsB α (Fig. 4A). Like PmScsB α subdomain A, *E. coli* DsbD α has two catalytic cysteines and a β -hairpin close to the active site, but it does not have the $\beta 2$ - $\beta 3$ loop of PmScsB α . Two other hits in the DALI search were the mouse γ -adaptin appendage domain from clathrin-binding adaptor AP-1 (Protein Data Bank code 2A7B; r.m.s.d., 2.4 Å, 106 residues aligned) and the GAE domain of the clathrin-binding adaptor GGA protein from *Saccharomyces cerevisiae* (Protein Data Bank code 3MNM; r.m.s.d., 2.4 Å, 102 residues aligned) (Fig. 4, B and C). These proteins have typical immunoglobulin-like folds with no catalytic cysteines, and like EcDsbD α they have one immunoglobulin fold that aligns with subdomain A of PmScsB α . These three proteins were also hits in a DALI search against PmScsB α subdomain B although with much higher r.m.s.d. values (Protein Data Bank code 1JPE: r.m.s.d., 3.8 Å, 75 residues aligned; Protein Data Bank code 2A7B: r.m.s.d., 3.0 Å,

84 residues aligned; Protein Data Bank code 3MNM: r.m.s.d., 2.9 Å, 86 residues aligned). Curiously, there were no high-scoring DALI hits that had a tandem immunoglobulin-fold arrangement like that of PmScsB α . We did find lower-scoring DALI hits with two immunoglobulin-like folds (mostly antigen-binding fragments of antibodies; e.g. Protein Data Bank code 5JUE; Z-score, 4.6; r.m.s.d., 3.0 Å, 80 residues aligned), but they lacked the connecting α -helix of PmScsB α .

Structure-based sequence alignment

The amino acid sequence of PmScsB α was aligned with that of EcDsbD α using structure-based alignment and the sequences of CcScsB α and StScsB α (Fig. 5). ScsB α from *S. enterica* Typhimurium and *C. crescentus* were chosen as these are the only other organisms where the interaction partner, ScsC, has been characterized. EcDsbD α was chosen because of the known structural and functional relationship. PmScsB α shares 44% sequence identity with StScsB α (280 residues), 21% identity with CcScsB α (291 residues), and just 12%

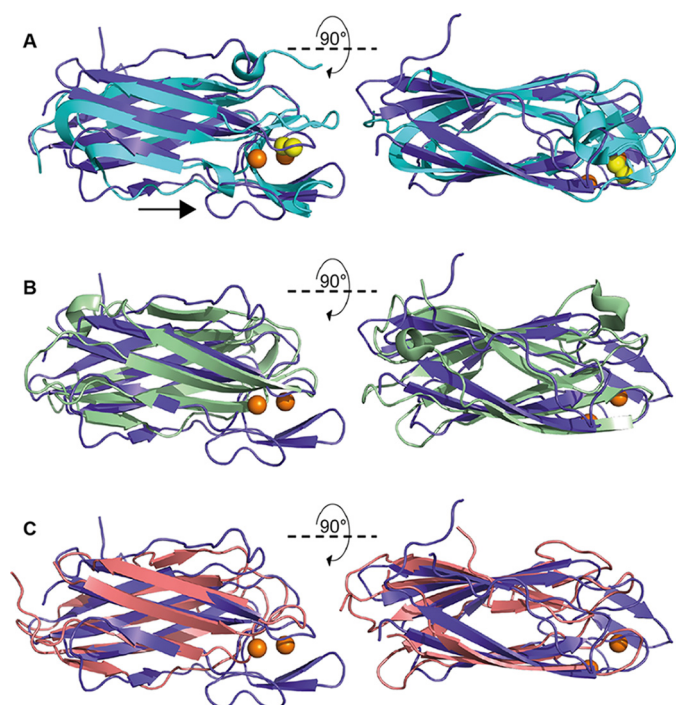


Figure 4. Structural overlay of PmScsB α subdomain A with selected DALI hits. A, PmScsB α subdomain A (purple) aligned with EcDsbD α (Protein Data Bank code 1JPE) (cyan). The catalytic cysteines of both PmScsB α subdomain A and EcDsbD α are shown as spheres and colored in orange and yellow, respectively. An arrow indicates the extended loop in the PmScsB α structure. B, PmScsB α subdomain A (purple) aligned with Protein Data Bank code 2A7B (light green). C, PmScsB α subdomain A (purple) aligned with Protein Data Bank code 3MNM (light pink). Neither 2A7B nor 3MNM have catalytic cysteines so in both B and C the orange spheres correlate to the cysteines of PmScsB α .

identity with EcDsbD α (116 residues of Protein Data Bank code 1JPE). There are several conserved residues across the three ScsB α and EcDsbD α protein sequences aside from the catalytic cysteines. Other conserved residues include Leu³⁴ and Ile⁵⁸ (PmScsB α numbering); their side chains interact with each other in the hydrophobic core of both PmScsB α and EcDsbD α so their conservation suggests a key role in folding or stability. Interestingly, the tyrosine hydroxyl of the conserved residue Tyr⁴⁵ (Tyr⁴² in EcDsbD α) is within 3.5–3.8 Å of the active-site sulfurs of Cys¹¹⁴ and Cys¹¹⁸, suggesting a potential role in catalysis or substrate binding. Two other conserved residues, Tyr⁸⁷ and Pro⁷², are located at either end of the β -hairpin. The hydroxyl group of Tyr⁸⁷ is within hydrogen-bonding distance of the main-chain oxygen of Pro⁷² (~2.6 Å), suggesting that their conservation may be important in preserving the structure of the β -hairpin. The β 2- β 3 loop sequence is also highly conserved across the ScsB α sequences, suggesting an important function.

Formation of a 3:1 PmScsC–PmScsB α complex

The interaction between the catalytic cysteines of PmScsC and PmScsB α is transient. For this reason, the catalytic cysteine variants PmScsC C87S and PmScsB α C114A were produced. These variants allowed the capture of a stable PmScsC–PmScsB α complex for structural studies. Size exclusion chromatography (SEC) and subsequent SDS-PAGE analysis suggested that the predominant complex species had a 3:1 ratio of PmScsC to PmScsB α , corresponding to one PmScsC trimer bound to one PmScsB α monomer (Fig. 6). The predicted

molecular mass calculated from SAXS and SANS analysis (Table 2) also provided evidence to support this stoichiometry. A peak corresponding to a larger species was seen on the SEC chromatogram (Fig. 6A, peak marked Z), suggesting that a smaller amount of 3:2 and/or 3:3 complex may have also formed.

SAXS and SANS provide structural insights into the PmScsC–PmScsB α interaction

SANS contrast variation experiments were performed on the 3:1 PmScsC–PmScsB α complex formed using unlabeled PmScsC C87S and deuterium-labeled PmScsB α C114A (^DPmScsB α C114A) (Fig. 7). Deuterium labeling changes the neutron scattering length density of PmScsB α . It is possible to tune the neutron scattering length density of the solvent by changing its deuterium content such that it matches one of the components of the protein complex. This is said to be the match point of that component, and the measured scattering data can then be interpreted as being from the unmatched component of the complex alone. Data collected close to the ^DPmScsB α C114A match point (100% D₂O, where PmScsC C87S dominates the scattering) indicate that the highly dynamic PmScsC protein becomes comparatively rigid and adopts a conformation that, at low-resolution, appears symmetrical upon interaction with PmScsB α . Specifically, the pair-distance distribution function ($p(r)$) is bimodal (Fig. 8A, green curve) with two well defined peaks and similar to the $p(r)$ generated from the extended symmetrical crystal structure (Protein Data Bank code 5ID4) (Fig. 8A, black dashed curve) (10). An asymmetric arrangement of the PmScsC trimer would yield an asymmetrically shaped second peak in the $p(r)$, whereas significant flexibility would see this same peak broaden.

Analysis of the SANS data showed that a plot of the scattering intensity at zero angle ($I(0)$) normalized by protein concentration versus deuterium content of the solvent was well represented by a parabolic function, indicating that the samples were pure (Fig. 8B). A Stuhmann plot revealed that the ^DPmScsB α C114A molecule was located toward the center of the complex (Fig. 8C). A rigid body model of the complex was optimized simultaneously against the SAXS data set and five SANS contrast variation data sets. The resulting model provided an excellent fit to all of the scattering data (Fig. 9A). The configuration adopted by PmScsB α and PmScsC in the model precludes the simultaneous binding of two (or three) PmScsB α molecules to PmScsC, helping to explain the preferential formation of a trimer–monomer complex (Fig. 6). The model also highlights two potential interfaces between PmScsC and PmScsB α (Fig. 9A). The most obvious interface is that between chain A of PmScsC and subdomain A of PmScsB α for which the intermolecular disulfide bond is modeled. The resolution of the model is too low to be definitive, but the interface includes residues that could form hydrogen bond interactions. The second interface is between chain A of PmScsC and subdomain B (the second immunoglobulin domain) of PmScsB α .

Discussion

Suppressor of copper sensitivity proteins play a role in the response to copper stress of the important human pathogens *S. enterica* Typhimurium and *P. mirabilis* (7, 10). At least two of

P. mirabilis ScsB α and ScsC form a functional redox relay

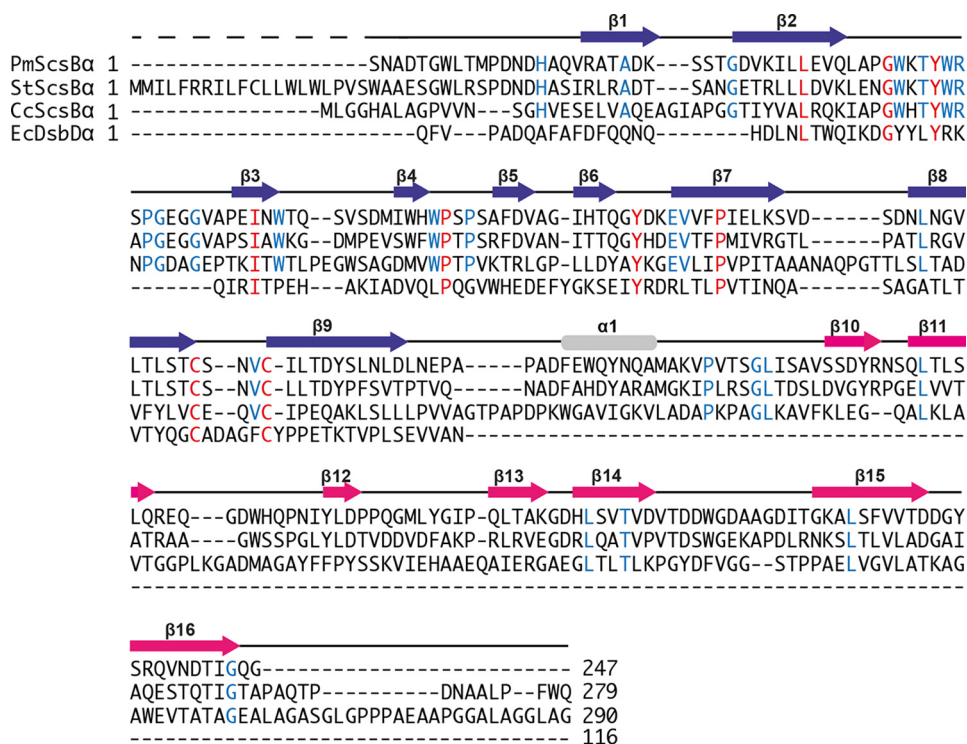


Figure 5. Sequence alignments. The sequence alignment of the PmScsB α crystal structure with StScsB α and CcScsB α sequences and the structure-based sequence alignment with EcDsbD α crystal structure (Protein Data Bank code 1JPE) are shown. Secondary structure elements of PmScsB α are shown above the corresponding sequence and are colored according to the scheme in Fig. 3. Residues that are conserved between all four proteins are highlighted in red; those that are conserved only between the ScsB α proteins are colored blue.

the four Scs proteins are homologues of Dsb proteins (6), which are essential for the correct formation of disulfide bonds in virulence factors of many Gram-negative bacteria (14–17). *P. mirabilis* ScsC was recently shown to be a trimeric, highly dynamic disulfide isomerase (10). The present study aimed to characterize PmScsB α , the predicted interaction partner of PmScsC, and to investigate the nature of the interaction between the two.

The domain architecture of full-length ScsB resembles that of *E. coli* DsbD, the major difference being the size of the periplasmic N-terminal domain. This difference suggested that ScsB α would be structurally distinct from DsbD α perhaps because they interact with different substrates. We confirmed that PmScsC and PmScsB α are redox partners and are therefore functionally similar to EcDsbC and EcDsbD α . We also reported the structure of PmScsB α , showing that it consists of two immunoglobulin-like folds connected by an α -helix. The structures of the two immunoglobulin-like subdomains of PmScsB α are broadly similar with the exception that subdomain A has a catalytic CXXXC motif as well as a β -hairpin and extended loop that both cover the CXXXC active site. The positioning of the β -hairpin and the loop could potentially shield the active site from nonspecific interactions or facilitate interactions with partner proteins. Unexpectedly, we found that domain A of PmScsB α shares the same features of the immunoglobulin fold of EcDsbD α (Fig. 4; r.m.s.d., 2.5 Å, 103 residues aligned) despite a sequence identity of just 12%. The key difference between the structures of subdomain A and EcDsbD α is that EcDsbD α lacks the β 2- β 3 loop of PmScsB α . The sequence of this β 2- β 3 loop is conserved in *S. enterica* Typhimurium and *C. crescentus* ScsB α , suggesting that it plays a

key functional role. A residue that is conserved across the three ScsB α s and EcDsbD α is Tyr⁴⁵ (PmScsB α numbering). In EcDsbD α , the equivalent Tyr⁴² hydroxyl is thought to be involved in nucleophilic attack of Cys¹⁰³, which resolves the intermolecular disulfide formed between EcDsbD α and its substrate (e.g. EcDsbC) (18). The nucleophilic attack in EcDsbD α is proposed to also require Asp⁶⁸ (18), a residue that is not conserved in Pm-, Cc-, or StScsB α . It is unclear from the PmScsB α structure which residue, if any, might play a role equivalent to that of Asp⁶⁸.

The discovery of tandem immunoglobulin-like folds in PmScsB α raises the question as to the function of the second or noncatalytic immunoglobulin-like fold. EcDsbD α has a single immunoglobulin-like fold, which, in the *E. coli* DsbC-DsbD α crystal structure, spans the central cleft of the V-shaped DsbC substrate to interact with both domains of the disulfide isomerase (Fig. 9B) (19). This binding mode is thought to favor binding to dimeric EcDsbC; EcDsbD α is unable to interact with monomeric EcDsbC (3, 19). By comparison, the SANS-derived model of the PmScsC-PmScsB α complex suggests that PmScsB α subdomain A interacts with just one of the three PmScsC protomers in the trimer. Subdomain B of PmScsB α forms a secondary binding site to PmScsC that may stabilize the primary interaction or add specificity (Fig. 9A). Subdomain B could also be required for interactions with other proteins that have yet to be identified.

EcDsbC-EcDsbD α is the redox relay complex formed between dimeric EcDsbC and monomeric EcDsbD α . The crystal structure revealed a 2:1 (rather than a 2:2) complex between the dimer of EcDsbC and a monomer of EcDsbD α (3, 19). On this basis, we hypothesized that PmScsC-PmScsB α would form a 3:1 complex between trimeric PmScsC and monomeric

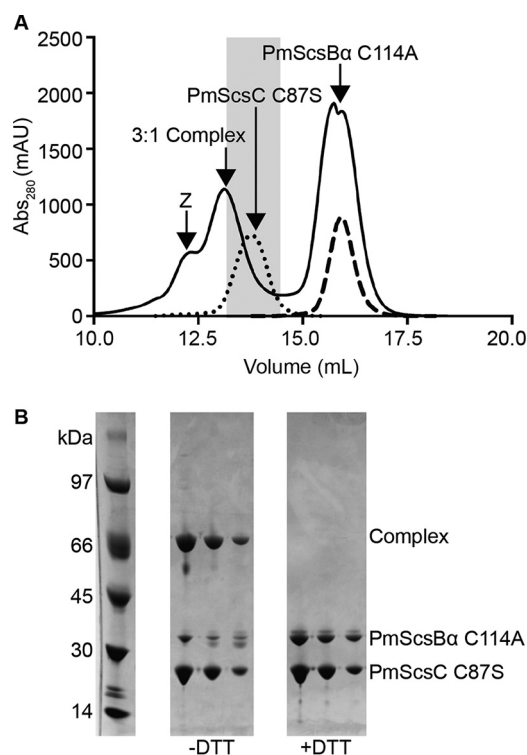


Figure 6. Formation of 3:1 PmScsC C87S–PmScsB α C114A complex. *A*, SEC chromatographs from the purification of the 3:1 PmScsC–PmScsB α complex (solid line), purified PmScsC C87S (dotted line), and PmScsB α C114A (dashed line). In the purification of the complex, excess PmScsC was removed prior to SEC using an immobilized metal ion affinity chromatography step. The leading shoulder (Z) suggests the presence of a 3:2 and/or 3:3 PmScsC C87S–PmScsB α C114A complex. The shaded region highlights the fractions of the 3:1 PmScsC–PmScsB α peak (solid line) that were pooled for structural analysis. *B*, the fractions from the shaded region of the 3:1 PmScsC–PmScsB α complex peak run on SDS-PAGE without and with DTT. PmScsC is a trimer that separates and runs as a monomer on SDS-PAGE. The lane labeled –DTT shows that the trimer–monomer complex separates into complex (covalently linked protomer of PmScsC with monomer of PmScsB α ; 55.1 kDa) and uncomplexed PmScsC C87S (24.8 kDa) in an approximate 1:1 ratio. When run with DTT (lane labeled +DTT), the higher band dissociates into the two complex components in an approximate 3:1 ratio. Abs, absorbance; mAU, milliabsorbance units.

PmScsB α , and the SANS structure of the complex appears to preclude higher stoichiometry. Nevertheless, we did find *in vitro* evidence suggestive of PmScsC forming 3:2 and 3:3 complexes with PmScsB α (Fig. 6A), showing that different arrangements might form with PmScsB α in the absence of the PmScsB β - and γ -domains. We expect that these higher order complexes would not form in the context of full-length PmScsB.

How do our findings on PmScsB α and PmScsC inform on interactions between ScsC and ScsB in other organisms? A functional interaction between ScsC and ScsB has already been reported for *C. crescentus* (5). With two examples now confirmed, the ScsB–C redox relay system is likely to be present in all organisms that encode the four-gene *scs* cassette. However, there is likely to be a wide diversity of interactions. ScsC is reported to be monomeric for StScsC (7), dimeric for CcScsC (5), and trimeric for PmScsC (10). By contrast, ScsB shares similar features across the same organisms, suggesting that StScsB α and CcScsB α both incorporate the tandem immunoglobulin-fold arrangement present in PmScsB α . As indicated above, both subdomains of PmScsB α interact with one PmScsC protomer, suggesting that this tandem immunoglobulin-fold

arrangement could facilitate the interaction with ScsCs regardless of the ScsC oligomeric state. Future studies will be needed to establish whether it is the tandem immunoglobulin-fold architecture that permits interactions with monomeric, dimeric, and trimeric PmScsCs. Curiously, a BLAST search of *E. coli* DsbD or *S. enterica* Typhimurium DsbD against the *P. mirabilis* genome did not identify any hits, suggesting the possibility that PmScsB may also act as the redox partner for *P. mirabilis* DsbC proteins.

Experimental procedures

Sequence analysis

The TMHMM Server (version 2.0) was used to determine the region of the ScsB proteins that formed the N-terminal periplasmic domain. EMBOSS Needle (20, 21) with residues 1–275, 1–279, and 1–290 of UniProt entries B4EV20 (PmScsB), AAL20046 (StScsB), and Q9ABL0 (CcScsB), respectively, was used to calculate the sequence identities reported among these proteins. The DALI server (13) was used to calculate r.m.s.d. values and structure-based sequence identities. Coot (22) was used to create visuals of the structural alignments. The sequences of all four proteins were aligned using PROMALS3D (23) with the Protein Data Bank files of PmScsB α and EcDsbD α (code 1JPE) instead of the sequence alone. Residue numbers quoted in the text were taken from the deposited Protein Data Bank files for the PmScsC and PmScsB α protein structures, which are numbered based on the tobacco etch virus protease-cleaved protein sequence (starting S¹N²A³...).

Molecular biology

A codon-optimized gene encoding *P. mirabilis* ScsB α without the predicted signal peptide (UniProt entry B4EV20, residues 21–275; Integrated DNA Technologies) was inserted into pMCSG7 (24) using ligation-independent cloning. The PmScsC (UniProt entry C2LPE2/B4EV21) construct used throughout this study was created previously (10). The constructs for the variants PmScsC C87S and PmScsB α C114A were created using the QuikChange[®] Lightning site-directed mutagenesis kit (Agilent Technologies). The WT PmScsC and PmScsB α constructs were used as templates, and primers 5′-gcggatcgaaacgttagagtacgggcaattatag-3′, 5′-ctataattgccgta-ctctaaacgtttcgatccg-3′, 5′-gtcagaatgcatacattgctagcggctactcaat-gtaaggacacc-3′, and 5′-ggtgtccttacattgattaccgtagcaatgtatgc-attctgac-3′, respectively, were used to introduce the point mutations. PmScsB α was also subcloned into pET24a for deuterated bioreactor expression using restriction enzymes EcoRI and NdeI. All constructs contained an N-terminal His₆ tag followed by a tobacco etch virus protease cleavage site and were confirmed by sequencing.

Protein production

Except for the selenomethionine-labeled PmScsB α and deuterated PmScsB α C114A, all proteins were expressed and purified as outlined previously (10). The redox state of the cysteines was confirmed spectrophotometrically with 5,5′-dithiobis(2-nitrobenzoic acid) (Ellman’s reagent) as described previously (25). Yields for PmScsC and PmScsB α derivatives were around

P. mirabilis ScsB α and ScsC form a functional redox relay

Table 2

SAS data collection and analysis details for the PmScsC–PmScsB α complex

ANSTO, Australian Nuclear Science and Technology Organisation; %_S, percentage of D₂O in the sample; %_B, percentage of D₂O in the buffer.

	SAXS	SANS
Data collection parameters		
Instrument	SAXS-WAXS (Australian Synchrotron)	QUOKKA (ANSTO)
Beam geometry	Point	Point
Wavelength (Å)	1.033	5.00
Sample to detector distance (m)	2.680	2.000 (short); 10.000 (long)
q -range (Å ⁻¹)	0.007–0.35	0.03–0.40 (short); 0.01–0.09 (long)
Exposure time (s)	13 (13 × 1-s exposures)	0% ^S , 7,200; 20% ^S , 10,800; 42% ^S , 21,600; 80% ^S , 7,200; 100% ^S , 3,600; 0% ^B , 10,800; 100% ^B , 7,200
Measurement type	Concentration series from 96-well plate; 1.0-mm quartz capillary	Neutron contrast variation; Hellma 120-QS 1.0-mm quartz cells
Protein concentration range (mg/ml)	0.56–4.50	
Temperature (K)	283	289
Absolute intensity calibration	Water	Incident beam intensity
Sample details		
Extinction coefficient (A_{280} , 0.1%, w/v)	0.979	0.979
Partial specific volume (cm ³ g ⁻¹)	0.737	0.737
Contrast, $\Delta\rho$ (10 ¹⁰ cm ⁻²)	2.86	3.36 (0%); 2.23 (20%); 1.10 (42%); -1.17 (80%); -2.30 (100%)
Molecular mass (from sequence) (kDa)	105.5	105.5
Protein concentration (mg/ml) ^a	0.56	5.30 (0% ^S); 5.20 (20% ^S); 5.10 (42% ^S); 5.00 (80% ^S); 4.90 (100% ^S)
Structural parameters		
$I(0)$ (cm ⁻¹) (from Guinier)	0.04060 ± 0.00010	
R_g (Å) (from Guinier)	39.2 ± 0.2	
$I(0)$ (cm ⁻¹) (from $p(r)$)	0.04026 ± 0.00010	0.5020 ± 0.0019 (0%); 0.2217 ± 0.0013 (20%); 0.0357 ± 0.0007 (42%); 0.0561 ± 0.0008 (80%); 0.2211 ± 0.0010 (100%)
R_g (Å) (from $p(r)$)	38.7 ± 0.1	36.3 ± 0.2 (0%); 34.6 ± 0.3 (20%); 24.3 ± 1.1 (42%); 35.6 ± 0.5 (80%); 37.0 ± 0.2 (100%)
D_{max} (Å)	115 ± 3	110 ± 3
Porod volume (Å ³)	131,300 ± 7,000	116,000 ± 6,000 ^b
Molecular mass determination		
Molecular mass from $I(0)$ (kDa)	97 ± 5	95 ± 5 ^b
Molecular mass from Porod (kDa)	108 ± 5	95 ± 5

^a $I(0) = 0.0854 \pm 0.0002$ cm⁻¹, $R_g = 39.0 \pm 0.1$ Å, $M = 103 \pm 5$ kDa (1.13 mg/ml); $I(0) = 0.1779 \pm 0.0002$ cm⁻¹, $R_g = 39.0 \pm 0.1$ Å, $M = 107 \pm 5$ kDa (2.25 mg/ml); $I(0) = 0.3476 \pm 0.0003$ cm⁻¹, $R_g = 38.8 \pm 0.1$ Å, $M = 105 \pm 5$ kDa (4.50 mg/ml). There is a small systematic change in R_g but no systematic change in M ; thus, it was deemed that the complex is largely free of concentration-dependent effects up to a concentration of ~5.0 mg/ml.

^b The Porod volume calculation is not valid for systems where the $\Delta\rho$ of the particle is not homogeneous (such as is the case for the neutron contrast variation experiment reported here). Instead, the composite scattering functions (Fig. 8D) were summed together to give the scattering curve of the protein complex with homogeneous contrast (*i.e.* $I_{\text{homogeneous}} = I_{11} + I_{22} + I_{12}$), and the Porod volume was determined from this curve. The molecular mass derived from the $I(0)$ was also taken from this curve.

80 and 40 mg/liter of culture (~15 g cell weight harvested), respectively. SDS-PAGE (NuPAGE® system, 4–12% BisTris gel, Invitrogen) with Coomassie Blue stain was used to assess the protein quality.

Expression of SeMet-labeled PmScsB α

To express SeMet-labeled PmScsB α , needed for experimental phasing in crystallographic structure determination, a 10-ml starter culture of *E. coli* BL21 (DE3) pLysS cells containing pMCSG7-PmScsB α was grown in LB medium supplemented with the appropriate antibiotics at 37 °C for 4–5 h at 220 rpm. This culture was then used to inoculate 1 liter of M9 minimal medium supplemented with antibiotics and amino acids (100 mg of L-methionine, L-lysine, L-threonine, and L-phenylalanine and 50 mg of L-leucine, L-isoleucine, and L-valine) and then incubated overnight at 37 °C at 220 rpm. Cells were harvested from the overnight culture, washed with 1 liter of sterile water, and resuspended in water to an A_{600} of ~1. M9 minimal medium containing antibiotics but no amino acids was then inoculated with the cells to a final A_{600} of 0.1. The cells were cultured at 30 °C at 220 rpm for 6–8 h until an A_{600} of 0.5 was reached. Amino acids, including 100 mg of L-selenomethionine instead of L-methionine, were then added to the culture flasks, and after 15 min at 30 °C isopropyl 1-thio- β -D-galactopyranoside was added to a final concentration of 1 mM to induce expression. The cultures were incubated at 30 °C at 220 rpm

overnight. Cells were harvested, and the protein was purified as described previously (10) with the addition of 5 mM DTT to all purification buffers. The yield of SeMet-labeled PmScsB α was 5 mg/liter of culture (~5 g of cell pellet).

Expression of deuterated PmScsB α C114A

Deuterated PmScsB α C114A was expressed for SANS analysis of the complex between PmScsC C87S and PmScsB α C114A. The deuterated protein PmScsB α C114A was produced at the National Deuteration Facility, Australian Nuclear Science and Technology Organisation in 1 liter of “ModC1” medium (26) containing 90% (v/v) D₂O and unlabeled glycerol (40 g/liter). Miniprep plasmid DNA “pET24a-PmScsB α C114A” was used to transform 50 μ l of Invitrogen competent BL21*(DE3) cells, which were then incubated with 250 μ l of SOC medium for 2 h. The 300- μ l culture was added to 10 ml of ModC1 medium containing 50% D₂O and 40 μ g/ml kanamycin, shaking at 200 rpm at 37 °C. After 16 h (A_{600} , 1.2), 9 ml was added to 36 ml of fresh medium with kanamycin at 100% D₂O (*i.e.* 45 ml at 90% D₂O). After another 5 h (A_{600} , 0.9), the culture was diluted with fresh 90% D₂O medium to 102 ml. After another 5 h, 100 ml (A_{600} , 0.87) was used to inoculate 900 ml of fresh 90% D₂O medium with kanamycin in a 2-liter Real Time Engineering bioreactor aerated with air at 0.5 liter/min and with pH held to a minimum of 6.2 by addition of 28% NH₄OH in H₂O (Sigma). Dissolved oxygen tension was set to 75% and was

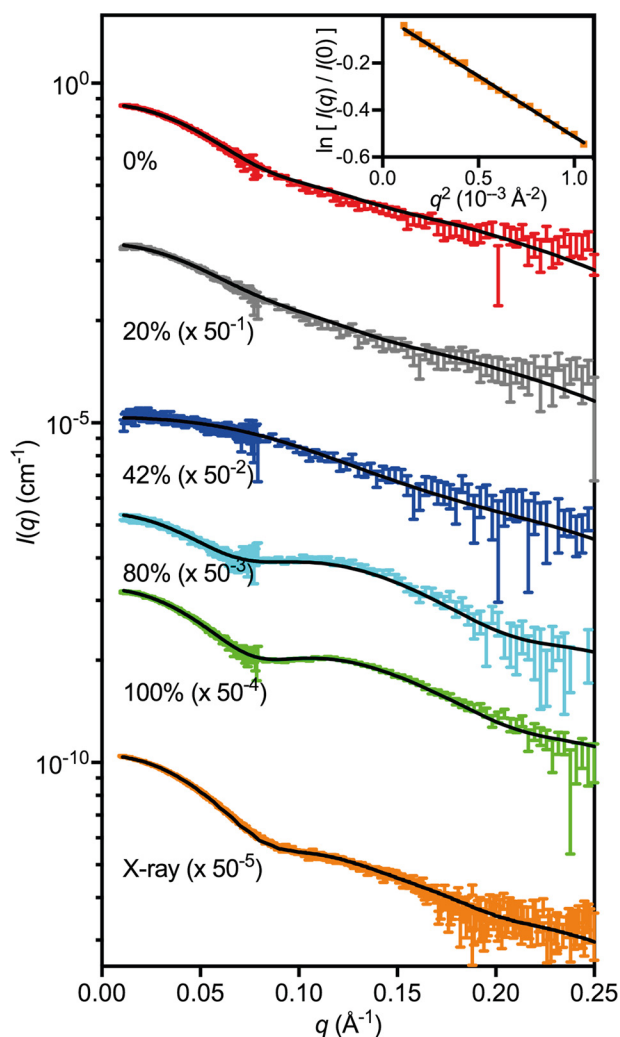


Figure 7. SAXS/SANS scattering curves. SAXS and SANS data (offset for clarity) collected from the 3:1 PmScsC C875–^DPmScsB α C114A complex with the model scattering curves overlaid (solid black line): 0% ($\chi^2 = 1.16$; red; on absolute scale), 20% ($\chi^2 = 1.20$; gray; offset by a factor of 50^{-1}), 42% ($\chi^2 = 1.00$; blue; offset by a factor of 50^{-2}), 80% ($\chi^2 = 1.11$; cyan; offset by a factor of 50^{-3}), 100% ($\chi^2 = 0.86$; green; offset by a factor of 50^{-4}), and X-ray ($\chi^2 = 1.80$; orange; offset by a factor of 50^{-5}). A Guinier plot for the SAXS data is shown in the inset. The match point of PmScsC C875 is $\sim 42\%$ D₂O (blue) where ^DPmScsB α C114A dominates the scattering, whereas the match point of ^DPmScsB α C114A is $\sim 100\%$ D₂O (green) where PmScsC C875 dominates the scattering. Error bars represent the S.E.

above 60% throughout. At an A_{600} of 14.2, the temperature was lowered to 20 °C, and expression was induced by the addition of 1 mM isopropyl 1-thio- β -D-galactopyranoside. At 17 h postinduction, with an A_{600} of 32, the culture was harvested with a wet weight yield of 79.4 g and with excellent expression as evident by SDS-PAGE. The deuteration level was determined by partial trypsin digest MALDI-TOF comparison of unlabeled and labeled samples and was found to be 70.8%. Deuterated PmScsB α C114A was purified as described for the unlabeled protein except the His₆ tag was not cleaved as it was needed for the purification of the complex. The yield of purified deuterated PmScsB α was ~ 240 mg/liter of bioreactor culture (~ 40 g of cell pellet).

Determination of protein concentration

The reported protein concentrations were determined using the A_{280} of the sample (read using a Thermo Scientific Nano-

Drop 2000c spectrophotometer) and calculated extinction coefficients from ProtParam (27).

Crystal structure of PmScsB α

A number of conditions from commercial screens resulted in PmScsB α crystals. These conditions were replicated in 24-well plates, and the best diffracting SeMet-labeled PmScsB α crystals were obtained in a drop containing 1 μ l of 43 mg/ml protein in 10 mM HEPES, pH 7.4, 5 mM DTT and 1 μ l of 0.1 M MES monohydrate, pH 6, 6% (v/v) Tacsimate, pH 6, 24% PEG 4000. A commercial additive screen (Hampton Research) was used to optimize crystals, and those grown over 2 days to ~ 400 μ m with the addition of 4% 2,5-hexanediol or 4% 1,3-butanediol resulted in the best diffraction. Crystals were cryoprotected in the crystallization condition plus 20% glycerol and flash frozen in liquid nitrogen.

Because of the lack of a suitable model for molecular replacement, experimental phasing was required to solve the crystal structure of PmScsB α . A fluorescence scan was used to determine the absorption edge of SeMet-labeled crystals, and a data set (Table 1) was collected near the peak absorption wavelength (0.9786 Å) at 100 K. Data processing in autoPROC (28), which utilizes XDS (29) and AIMLESS (30), determined the space group to be P2₁2₁2₁. SAD phasing using the SHELX workflow (31) in HKL2MAP (32) found 14 selenium sites with an occupancy >0.2 . We expected only 12 selenium sites; the extra two sites were positioned very close to other sites, suggesting alternate conformations, although only one SeMet was modeled with an alternate conformation in the final structure. SAD phasing resulted in an initial incomplete alanine model of the protein structure (figure of merit, 0.42). This initial model was then used for molecular replacement against the same data in Phaser (33) in the CCP4 suite (34). Two rounds of automated building and refinement using Buccaneer (35) with REFMAC (36), as implemented in CCP4 (34), completed the structure, revealing three molecules in the asymmetric unit. Then several rounds of manual adjustment in Coot (22) and refinement in PHENIX (37) were performed with reference to the validation program MolProbity (38). Multiple residues in the crystal structure have alternate conformers, and occupancies of the selenium atoms in the SeMet residues were all <1.0 . The electron density for some loop regions is poor in chains B and C, particularly residues 79–82, 99–100, and 51–52 (chain B only). R/R_{free} values are 17.3 and 19.8% at a resolution of 1.54 Å. All structural figures were made in PyMOL (39).

Redox interaction assay

To confirm the redox interaction between PmScsC and PmScsB α , oxidized PmScsC and reduced PmScsB α were incubated together at final concentrations of 10 μ M in 100 mM sodium phosphate, pH 7, 1 mM EDTA for 2 h. As controls, oxidized and reduced forms of both proteins, a sample containing reduced PmScsC and oxidized PmScsB α , and a sample with oxidized PmScsC with PmScsB α C114A were also incubated for 2 h. All samples were then treated with 10% TCA to precipitate the protein, and after centrifugation the pellets were washed with 100% cold acetone and dried. The protein pellets were resuspended in a solution of 200 μ M AMS in 1% SDS, 50 mM Tris, pH 7.0. AMS binds to the reduced cysteines of pro-

P. mirabilis ScsB α and ScsC form a functional redox relay

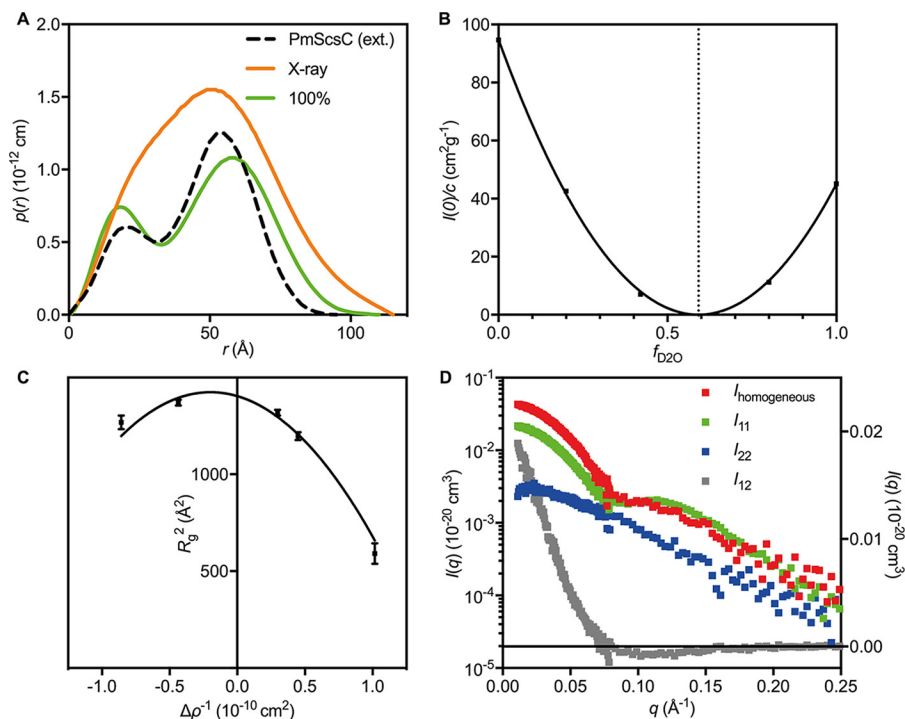


Figure 8. Other SAXS/SANS results. A, $p(r)$ derived from the experimental X-ray scattering data (orange) and the 100% scattering data (green), which should approximate the $p(r)$ for PmScsC C87S alone. The $p(r)$ derived from the extended (ext.) crystal structure (Protein Data Bank code 5ID4) is shown as a black dotted line for reference. B, a plot of $I(0)$ normalized by concentration as a function of D₂O content of the supporting solvent. The plot is parabolic in shape and reveals that the match point of the entire complex is 59% D₂O (vertical dotted line). C, Stuhrmann plot for the 3:1 PmScsC C87S–^DPmScsB α C114A complex, conforming to $R_g^2 = R_m^2 + \alpha\Delta\rho^{-1} - \beta\Delta\rho^{-2}$ where R_m is the radius of gyration of that object with homogenous contrast and α and β are related to the contrast variations within the object. The values obtained from a fit to the plot (solid black line) are: $R_m = 37.5 \pm 0.4$, $\alpha = -210 \pm 50$, and $\beta = 520 \pm 100$. The negative value of α reveals that the region with higher contrast (i.e. ^DPmScsB α C114A) lies toward the center of the molecule. Error bars represent the S.E. D, the composite scattering functions determined from the neutron contrast variation data. The I_{11} curve (green; left y axis) corresponds to scattering from PmScsC C87S, the I_{22} curve (blue; left y axis) corresponds to scattering from ^DPmScsB α C114A, and the I_{12} curve (gray; right y axis) is related to the arrangement of ^DPmScsB α C114A relative to PmScsC C87S. $I_{\text{homogeneous}} = I_{11} + I_{22} + I_{12}$ (red; left y axis) is the scattering curve of an object with the same shape as the PmScsC C87S–^DPmScsB α C114A complex but with homogeneous contrast and is used for estimating the Porod volume and molecular mass from the SANS data.

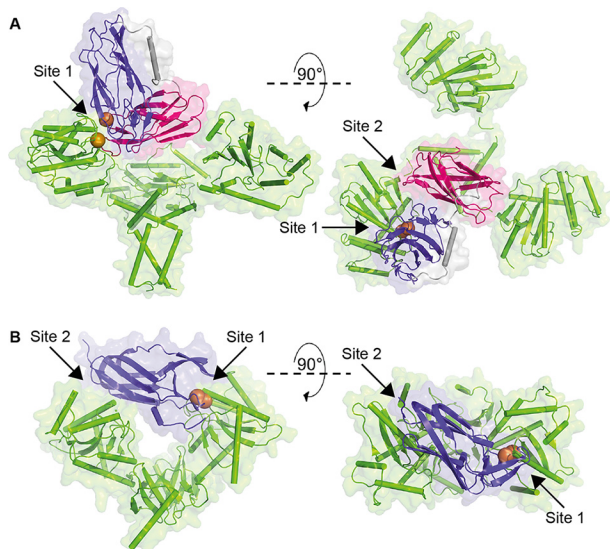


Figure 9. Binding sites in the PmScsC–PmScsB α SANS model and EcDsbC–EcDsbD α structure (Protein Data Bank code 1JZD). A, model of the 3:1 complex generated from the SAXS/SANS data shown in backbone and surface representation. PmScsB α binds to one PmScsC (green) protomer with both subdomains A (purple; Site 1) and B (magenta; Site 2). B, crystal structure of the EcDsbC–EcDsbD α complex. EcDsbD α (purple) binds to both protomers of EcDsbC (green; binding Sites 1 and 2). In both A and B, the catalytic cysteines involved in the intermolecular disulfide bond between the partner proteins are shown as orange spheres.

teins, increasing the molecular weight and allowing the differentiation between the oxidized and reduced forms of a protein when run on a gel. Therefore, all samples were run on a non-reducing, nondenaturing 12% NuPAGE BisTris gel for 2.5 h at 100 V. The gel was Coomassie-stained and imaged using an Odyssey[®] Fc imaging system (LI-COR[®] Biosciences) with the 700-nm channel.

RNase A isomerase assay

To determine whether PmScsB α activates the isomerase PmScsC, an isomerase assay utilizing scrambled RNase A (scrRNase A) and the RNase A model substrate cCMP was performed. Bovine RNase A (purchased from Sigma-Aldrich) was scrambled as described previously (40). The various oxidized and reduced protein samples described above for the gel-shift redox interaction assay were again prepared but with the addition of 40 μM scrRNase A to each sample. After 2 h, 50 μl of the protein/scrRNase A reactions was taken and added to 150 μl of 4 mM cCMP in a UV-Star 96-well plate (Greiner Bio-One, Austria). The increase in absorbance at 296 nm was monitored over 3 min with a Synergy H1 multimode plate reader (BioTek) and used to calculate the rate of cCMP hydrolysis. Native RNase A– and scrRNase A–only samples were included as controls and used to determine the relative activity of the RNase A in each

sample. The results shown are the average and S.D. of three technical replicates.

Complex formation

The PmScsC and PmScsB α cysteine variants were designed following the same approach used for the EcDsbC–EcDsbD α interaction (19). Mutation of cysteines in EcDsbC and EcDsbD α resulted in a stable complex between the two proteins (3). Cysteines Cys⁸⁷ of PmScsC and Cys¹¹⁴ of PmScsB α are the least accessible of the two cysteines in each active site, suggesting they facilitate resolution of intermolecular disulfide bonds. Variants PmScsC C87S and PmScsB α C114A were therefore prepared and used in complex formation studies.

The 3:1 PmScsC C87S–PmScsB α C114A complex was formed by mixing the two proteins together in a 3:1 ratio at concentrations of \sim 200 mg/ml and incubating the mixture at 37 °C for 3 days. To separate the complex and free PmScsB α from PmScsC, PmScsB α was left His-tagged, and the protein mixture was then run over 2 ml of fresh TALON resin twice. Columns were washed with 25 mM Tris, pH 7.4, 150 mM NaCl, and the complex and free PmScsB α were eluted with 25 mM Tris, pH 7.4, 150 mM NaCl, 250 mM imidazole. This was then run over a Superdex 200 10/300 Increase size exclusion column on an ÅKTA system to separate PmScsB α from complex. A peak on SEC eluted earlier than for ScsC, suggesting that a complex between the two proteins had formed (Fig. 6A). Running the fractions from the peak corresponding to the 3:1 complex on nonreducing SDS-PAGE resulted in three bands (Fig. 6B). The lower bands correlated to free PmScsC C87S (24.8 kDa) and a small amount of PmScsB α C114A (30.3 kDa), and the upper band corresponded to the molecular mass of one PmScsC C87S molecule bound to one PmScsB α C114A molecule (55.1 kDa). The upper band dissociated when reducing agent was added, leaving two bands correlating to monomeric PmScsC C87S and PmScsB α C114A in an approximate 3:1 ratio (Fig. 6B). There was also evidence for the formation of small amounts of complex containing PmScsC C87S and PmScsB α C114A in ratios of 3:3 and 3:2, but only those SEC fractions containing 3:1 complex were collected for further analysis. The complex formation process was repeated multiple times to gain enough sample for SAXS/SANS analysis as the overall yield of 3:1 complex was \sim 2.5%.

Small-angle solution scattering

Small-angle neutron scattering data shown in Table 2 were collected on the QUOKKA instrument at the Australian Nuclear Science and Technology Organisation (Table 2) (41). Two aliquots of PmScsC C87S–^DPmScsB α C114A complex at \sim 5 mg/ml were dialyzed, one against a buffer with a D₂O content of 0% and the other against a buffer with a D₂O content of \sim 100%. Samples with D₂O contents of 20, 42, and 80% were obtained by mixing the two original solutions at the appropriate ratios. The two-dimensional data were normalized to a common incident neutron count and corrected for sample transmission, background radiation, empty cell scattering, and detector sensitivity and radially averaged to produce $I(q)$ versus q profiles. Scattering data from the two different sample–detector distances were then merged, and buffer scattering data

were then subtracted from the protein + buffer data to give the protein scattering profiles (the 20, 42, and 80% buffer scattering curves were taken as a linear combination of the 0 and 100% buffer scattering curves). To correct for the effects of incoherent scattering by ¹H-rich samples, backgrounds levels were adjusted by a small constant such that the high- q scattering displayed q^{-4} dependence.

Small-angle X-ray scattering data were collected on the SAXS-WAXS beamline at the Australian Synchrotron (Table 2) (42). Serial dilutions of the stock solution of PmScsC C87S–^DPmScsB α C114A complex were made to give four concentrations between 0.55 and 4.5 mg/ml that were centrifuged at 10,000 \times g immediately before loading into a 96-well plate. To reduce radiation damage, samples (\sim 100 μ l) were drawn into a capillary from the 96-well plate and flowed past the beam. All measured two-dimensional data were averaged and corrected for sample transmission, solvent scattering, and detector sensitivity and radially averaged to produce $I(q)$ versus q profiles using Scatterbrain (version 2.7.1) (43).

The estimated molecular masses were calculated using values for contrast and partial specific volume predicted from the protein sequence using MULCh (version 1.1) (44). Data processing and Guinier analysis were performed using PRIMUS (version 3.2) (45). The $p(r)$ was generated from the experimental data using GNOM (version 4.6) (4) from which $I(0)$, R_g , and D_{\max} were determined. For the SANS data, analysis of the dependence of R_g upon contrast and calculation of the composite scattering functions were also calculated using MULCh (Fig. 8D). Corefinement of a rigid-body model against SANS and SAXS data was performed using SASREF (version 7.d) (46) where the crystal structure of PmScsC (Protein Data Bank code 4XVW, chain A) was broken into three rigid sections: 1) residues Ala³–Gln⁴³ were fixed to preserve the structure of the trimerization domain observed in the crystal structure, 2) residues Gln⁴⁴–Phe⁴⁷ were defined as a short linker with a restraint between residues Gln⁴³ and Gln⁴⁴ to keep them in close proximity, and 3) residues Arg⁴⁸–Lys²²⁴ were defined as the catalytic domain free to move with a restraint between residues Phe⁴⁷ and Arg⁴⁸ to keep them in close proximity. The additional PmScsC chains were generated by symmetry (assuming a C₃ point group). The crystal structure of PmScsB α (residues Ala²–Ala²⁴⁸) was included in the optimization with a distance restraint between Cys⁸⁴ of a PmScsC monomer and Cys¹¹⁸ of PmScsB α of 8 Å. Thus, although the complex overall is not symmetrical, the PmScsC portion of the model possesses 3-fold symmetry. The optimization was run 16 times, and the model that provided the best global fit to the scattering data is reported here; however, all models obtained are similar in structure.

Author contributions—E. J. F., F. K., and J. L. M. conceptualization; E. J. F., A. E. W., and J. L. M. data curation; E. J. F., F. K., and A. E. W. formal analysis; E. J. F., A. E. W., and J. L. M. validation; E. J. F., H. G. C., F. K., and A. E. W. investigation; E. J. F. and A. E. W. visualization; E. J. F., H. G. C., F. K., A. P. D., and A. E. W. methodology; E. J. F. writing-original draft; E. J. F., H. G. C., F. K., A. P. D., A. E. W., and J. L. M. writing-review and editing; H. G. C., F. K., A. E. W., and J. L. M. supervision; F. K., A. P. D., A. E. W., and J. L. M. resources; J. L. M. funding acquisition; J. L. M. project administration.

P. mirabilis ScsB α and ScsC form a functional redox relay

Acknowledgments—We acknowledge the support of the Australian Centre for Neutron Scattering, the National Deuterium Facility, and the SAXS-WAXS and MX beamlines at the Australian Synchrotron (Australian Nuclear Science and Technology Organisation), each partly supported by the National Collaborative Research Infrastructure Strategy – an initiative of the Australian Government, in providing the facilities used in this work. We thank the staff and facilities of the University of Queensland Remote Operation Crystallisation and X-ray (UQ ROCX) facility for support. We also acknowledge access to the University of Sydney Mass Spectrometry Core Facility, which was used to produce partial trypsin digest MALDI-TOF spectra. We thank Dr. Róisín M. McMahon and Signe Christensen for helpful discussions.

References

- Martin, J. L., Bardwell, J. C., and Kuriyan, J. (1993) Crystal structure of the DsbA protein required for disulfide bond formation *in vivo*. *Nature* **365**, 464–468 [CrossRef Medline](#)
- Inaba, K., Murakami, S., Suzuki, M., Nakagawa, A., Yamashita, E., Okada, K., and Ito, K. (2006) Crystal structure of the DsbB-DsbA complex reveals a mechanism of disulfide bond generation. *Cell* **127**, 789–801 [CrossRef Medline](#)
- Goldstone, D., Haebel, P. W., Katzen, F., Bader, M. W., Bardwell, J. C., Beckwith, J., and Metcalf, P. (2001) DsbC activation by the N-terminal domain of DsbD. *Proc. Natl. Acad. Sci. U.S.A.* **98**, 9551–9556 [CrossRef Medline](#)
- McCarthy, A. A., Haebel, P. W., Törrönen, A., Rybin, V., Baker, E. N., and Metcalf, P. (2000) Crystal structure of the protein disulfide isomerase, DsbC, from *Escherichia coli*. *Nat. Struct. Biol.* **7**, 196–199 [CrossRef Medline](#)
- Cho, S. H., Parsonage, D., Thurston, C., Dutton, R. J., Poole, L. B., Collet, J. F., and Beckwith, J. (2012) A new family of membrane electron transporters and its substrates, including a new cell envelope peroxidase, reveal a broadened reductive capacity of the oxidative bacterial cell envelope. *mBio* **3**, e00291–11 [CrossRef Medline](#)
- Gupta, S. D., Wu, H. C., and Rick, P. D. (1997) A *Salmonella typhimurium* genetic locus which confers copper tolerance on copper-sensitive mutants of *Escherichia coli*. *J. Bacteriol.* **179**, 4977–4984 [CrossRef Medline](#)
- Shepherd, M., Heras, B., Achard, M. E., King, G. J., Argente, M. P., Kurth, F., Taylor, S. L., Howard, M. J., King, N. P., Schembri, M. A., and McEwan, A. G. (2013) Structural and functional characterization of ScsC, a periplasmic thioredoxin-like protein from *Salmonella enterica* serovar Typhimurium. *Antioxid. Redox Signal.* **19**, 1494–1506 [CrossRef Medline](#)
- Edeling, M. A., Ahuja, U., Heras, B., Thöny-Meyer, L., and Martin, J. L. (2004) The acidic nature of the CcmG redox-active center is important for cytochrome *c* maturation in *Escherichia coli*. *J. Bacteriol.* **186**, 4030–4033 [CrossRef Medline](#)
- Edeling, M. A., Guddat, L. W., Fabianek, R. A., Thöny-Meyer, L., and Martin, J. L. (2002) Structure of CcmG/DsbE at 1.14 Å resolution: high-fidelity reducing activity in an indiscriminately oxidizing environment. *Structure* **10**, 973–979 [CrossRef Medline](#)
- Furlong, E. J., Lo, A. W., Kurth, F., Premkumar, L., Totsika, M., Achard, M. E. S., Halili, M. A., Heras, B., Whitten, A. E., Choudhury, H. G., Schembri, M. A., and Martin, J. L. (2017) A shape-shifting redox foldase contributes to *Proteus mirabilis* copper resistance. *Nat. Commun.* **8**, 16065 [CrossRef Medline](#)
- Krupp, R., Chan, C., and Missiakas, D. (2001) DsbD-catalyzed transport of electrons across the membrane of *Escherichia coli*. *J. Biol. Chem.* **276**, 3696–3701 [CrossRef Medline](#)
- Collet, J. F., Riemer, J., Bader, M. W., and Bardwell, J. C. (2002) Reconstitution of a disulfide isomerization system. *J. Biol. Chem.* **277**, 26886–26892 [CrossRef Medline](#)
- Holm, L., and Rosenström, P. (2010) Dali server: conservation mapping in 3D. *Nucleic Acids Res.* **38**, W545–W549 [CrossRef Medline](#)
- Ireland, P. M., McMahon, R. M., Marshall, L. E., Halili, M., Furlong, E., Tay, S., Martin, J. L., and Sarkar-Tyson, M. (2014) Disarming *Burkholderia pseudomallei*: structural and functional characterization of a disulfide oxidoreductase (DsbA) required for virulence *in vivo*. *Antioxid. Redox Signal.* **20**, 606–617 [CrossRef Medline](#)
- Heras, B., Shouldice, S. R., Totsika, M., Scanlon, M. J., Schembri, M. A., and Martin, J. L. (2009) DSB proteins and bacterial pathogenicity. *Nat. Rev. Microbiol.* **7**, 215–225 [CrossRef Medline](#)
- Miki, T., Okada, N., and Danbara, H. (2004) Two periplasmic disulfide oxidoreductases, DsbA and SrgA, target outer membrane protein SpiA, a component of the *Salmonella* pathogenicity island 2 type III secretion system. *J. Biol. Chem.* **279**, 34631–34642 [CrossRef Medline](#)
- Totsika, M., Heras, B., Wurple, D. J., and Schembri, M. A. (2009) Characterization of two homologous disulfide bond systems involved in virulence factor biogenesis in uropathogenic *Escherichia coli* CFT073. *J. Bacteriol.* **191**, 3901–3908 [CrossRef Medline](#)
- Goulding, C. W., Sawaya, M. R., Parseghian, A., Lim, V., Eisenberg, D., and Missiakas, D. (2002) Thiol-disulfide exchange in an immunoglobulin-like fold: structure of the N-terminal domain of DsbD. *Biochemistry* **41**, 6920–6927 [CrossRef Medline](#)
- Haebel, P. W., Goldstone, D., Katzen, F., Beckwith, J., and Metcalf, P. (2002) The disulfide bond isomerase DsbC is activated by an immunoglobulin-fold thiol oxidoreductase: crystal structure of the DsbC-DsbD α complex. *EMBO J.* **21**, 4774–4784 [CrossRef Medline](#)
- Rice, P., Longden, I., and Bleasby, A. (2000) EMBOSS: the European Molecular Biology Open Software Suite. *Trends Genet.* **16**, 276–277 [CrossRef Medline](#)
- Li, W., Cowley, A., Uludag, M., Gur, T., McWilliam, H., Squizzato, S., Park, Y. M., Buso, N., and Lopez, R. (2015) The EMBL-EBI bioinformatics web and programmatic tools framework. *Nucleic Acids Res.* **43**, W580–W584 [CrossRef Medline](#)
- Emsley, P., and Cowtan, K. (2004) Coot: model-building tools for molecular graphics. *Acta Crystallogr. D Biol. Crystallogr.* **60**, 2126–2132 [CrossRef Medline](#)
- Pei, J., Kim, B. H., and Grishin, N. V. (2008) PROMALS3D: a tool for multiple protein sequence and structure alignments. *Nucleic Acids Res.* **36**, 2295–2300 [CrossRef Medline](#)
- Stols, L., Gu, M., Dieckman, L., Raffin, R., Collart, F. R., and Donnelly, M. I. (2002) A new vector for high-throughput, ligation-independent cloning encoding a tobacco etch virus protease cleavage site. *Protein Expr. Purif.* **25**, 8–15 [CrossRef Medline](#)
- Walden, P. M., Halili, M. A., Archbold, J. K., Lindahl, F., Fairlie, D. P., Inaba, K., and Martin, J. L. (2013) The α -proteobacteria *Wolbachia pipiensis* protein disulfide machinery has a regulatory mechanism absent in γ -proteobacteria. *PLoS One* **8**, e81440 [CrossRef Medline](#)
- Duff, A. P., Wilde, K. L., Rekas, A., Lake, V., and Holden, P. J. (2015) Robust high-yield methodologies for ^2H and $^2\text{H}/^{15}\text{N}/^{13}\text{C}$ labeling of proteins for structural investigations using neutron scattering and NMR. *Methods Enzymol.* **565**, 3–25 [CrossRef Medline](#)
- Gasteiger, E., Hoogland, C., Gattiker, A., Duvaud, S., Wilkins, M. R., Appel, R. D., and Bairoch, A. (2005) Protein identification and analysis tools on the ExPASy server, in *The Proteomics Protocols Handbook* (Walker, J. M., ed) pp. 571–607, Humana Press, New York
- Vonrhein, C., Flensburg, C., Keller, P., Sharff, A., Smart, O., Paciorek, W., Womack, T., and Bricogne, G. (2011) Data processing and analysis with the autoPROC toolbox. *Acta Crystallogr. D Biol. Crystallogr.* **67**, 293–302 [CrossRef Medline](#)
- Kabsch, W. (2010) XDS. *Acta Crystallogr. D Biol. Crystallogr.* **66**, 12 [CrossRef](#)–132 [Medline](#)
- Evans, P. R., and Murshudov, G. N. (2013) How good are my data and what is the resolution? *Acta Crystallogr. D Biol. Crystallogr.* **69**, 1204–1214 [CrossRef Medline](#)
- Sheldrick, G. M. (2010) Experimental phasing with SHELXC/D/E: combining chain tracing with density modification. *Acta Crystallogr. D Biol. Crystallogr.* **66**, 479–485 [CrossRef Medline](#)
- Pape, T., and Schneider, T. R. (2004) HKL2MAP: a graphical user interface for macromolecular phasing with SHELX programs. *J. Appl. Crystallogr.* **37**, 843–844 [CrossRef](#)

33. McCoy, A. J., Grosse-Kunstleve, R. W., Adams, P. D., Winn, M. D., Storoni, L. C., and Read, R. J. (2007) Phaser crystallographic software. *J. Appl. Crystallogr.* **40**, 658–674 [CrossRef Medline](#)
34. Winn, M. D., Ballard, C. C., Cowtan, K. D., Dodson, E. J., Emsley, P., Evans, P. R., Keegan, R. M., Krissinel, E. B., Leslie, A. G., McCoy, A., McNicholas, S. J., Murshudov, G. N., Pannu, N. S., Potterton, E. A., Powell, H. R., *et al.* (2011) Overview of the CCP4 suite and current developments. *Acta Crystallogr. D Biol. Crystallogr.* **67**, 235–242 [CrossRef Medline](#)
35. Cowtan, K. (2006) The Buccaneer software for automated model building. 1. Tracing protein chains. *Acta Crystallogr. D Biol. Crystallogr.* **62**, 1002–1011 [CrossRef Medline](#)
36. Vagin, A. A., Steiner, R. A., Lebedev, A. A., Potterton, L., McNicholas, S., Long, F., and Murshudov, G. N. (2004) REFMAC5 dictionary: organization of prior chemical knowledge and guidelines for its use. *Acta Crystallogr. D Biol. Crystallogr.* **60**, 2184–2195 [CrossRef Medline](#)
37. Adams, P. D., Afonine, P. V., Bunkóczi, G., Chen, V. B., Davis, I. W., Echols, N., Headd, J. J., Hung, L. W., Kapral, G. J., Grosse-Kunstleve, R. W., McCoy, A. J., Moriarty, N. W., Oeffner, R., Read, R. J., Richardson, D. C., *et al.* (2010) PHENIX: a comprehensive Python-based system for macromolecular structure solution. *Acta Crystallogr. D Biol. Crystallogr.* **66**, 213–221 [CrossRef Medline](#)
38. Chen, V. B., Arendall, W. B., 3rd, Headd, J. J., Keedy, D. A., Immormino, R. M., Kapral, G. J., Murray, L. W., Richardson, J. S., and Richardson, D. C. (2010) MolProbity: all-atom structure validation for macromolecular crystallography. *Acta Crystallogr. D Biol. Crystallogr.* **66**, 12–21 [CrossRef Medline](#)
39. DeLano, W. L. (2015) *The PyMOL Molecular Graphics System*, version 1.6, Schrödinger, LLC, New York
40. Hillson, D. A., Lambert, N., and Freedman, R. B. (1984) Formation and isomerisation of disulfide bonds in proteins: protein disulfide-isomerase. *Methods Enzymol.* **107**, 281–294 [CrossRef Medline](#)
41. Gilbert, E. P., Schulz, J. C., and Noakes, T. J. (2006) ‘Quokka’—the small-angle neutron scattering instrument at OPAL. *Physica B Condens. Matter* **385–386**, 1180–1182
42. Kirby, N. M., Mudie, S. T., Hawley, A. M., Cookson, D. J., Mertens, H. D. T., Cowieson, N., and Samardzic-Boban, V. (2013) A low-background-intensity focusing small-angle X-ray scattering undulator beamline. *J. Appl. Crystallogr.* **46**, 1670–1680 [CrossRef](#)
43. Mudie, S. (2015) *Scatterbrain—software for acquiring, processing and viewing SAXS/WAXS data at the Australian Synchrotron*, Version 2.71, Australian Synchrotron, Clayton, Victoria, Australia
44. Whitten, A. E., Cai, S., and Trewhella, J. (2008) MULCh: modules for the analysis of small-angle neutron contrast variation data from biomolecular assemblies. *J. Appl. Crystallogr.* **41**, 222–226 [CrossRef](#)
45. Konarev, P. V., Volkov, V. V., Sokolova, A. V., Koch, M. H. J., and Svergun, D. I. (2003) PRIMUS: a Windows PC-based system for small-angle scattering data analysis. *J. Appl. Crystallogr.* **36**, 1277–1282 [CrossRef](#)
46. Petoukhov, M. V., and Svergun, D. I. (2005) Global rigid body modeling of macromolecular complexes against small-angle scattering data. *Biophys. J.* **89**, 1237–1250 [CrossRef Medline](#)